1521-0111/88/4/676–688$25.00
MOLECULAR PHARMACOLOGY

http://dx.doi.org/10.1124/mol.115.099911
Mol Pharmacol 88:676–688, October 2015

Substrate and Inhibitor–Specific Conformational Changes in the Human Serotonin Transporter Revealed by Voltage-Clamp Fluorometry[S]

Pella C. Söderhielm, Jacob Andersen, Lachlan Munro, Anne T. Nielsen, and Anders S. Kristensen

Department of Drug Design and Pharmacology, University of Copenhagen, Copenhagen, Denmark

Received May 13, 2015; accepted July 13, 2015

ABSTRACT

The serotonin transporter (SERT) regulates neurotransmission by the biogenic monoamine neurotransmitter serotonin (5-HT, 5-hydroxytryptamine) in the central nervous system, and drugs inhibiting SERT are widely used for the treatment of a variety of central nervous system diseases. The conformational dynamics of SERT transport function and inhibition is currently poorly understood. We used voltage-clamp fluorometry to study conformational changes in human SERT (hSERT) during 5-HT transport and inhibitor binding. Cys residues were introduced at 12 positions in hSERT to enable covalent attachment of a rhodamine-based fluorophore. Transport-associated changes in fluorescence from fluorophore-labeled hSERT expressed in *Xenopus* oocytes could be robustly detected at four positions in hSERT: endogenous Cys109 in the top of transmembrane domain (TM) 1b, Cys substituted for Thr323 in the top of TM6, Ala419 in the interface between TM8 and extracellular loop (EL) 4, and Leu481 in EL5. The reporter positions were used for time-resolved measurement of conformational changes during 5-HT transport and binding of cocaine and the selective serotonin reuptake inhibitors fluoxetine and escitalopram. At all reporter positions, fluorescence changes observed upon substrate application were distinctly different from those observed upon inhibitor application, with respect to relative amplitude or direction. Furthermore, escitalopram, fluoxetine, and cocaine induced a very similar pattern of fluorescent changes overall, which included movements within or around TM1b, EL4, and EL5. Taken together, our data lead us to suggest that competitive inhibitors stabilize hSERT in a state that is different from the apo outward-open conformation as well as inward-facing conformations.

Introduction

The serotonin transporter (SERT) regulates extracellular serotonin (5-HT, 5-hydroxytryptamine) concentration in the central nervous system by performing Na^+- and Cl^--coupled transport of 5-HT into neurons. Inhibitors of SERT are widely used for the treatment of psychiatric diseases, including selective serotonin reuptake inhibitors and tricyclic antidepressants. SERT belongs to the solute-carrier 6 (*SLC6*) transporter family together with neurotransmitter transporters for dopamine, norepinephrine, γ-aminobutyric acid, and glycine (Kristensen et al., 2011; Pramod et al., 2013). These operate by an alternating access mechanism, in which the transporter cycles between outward-facing, occluded and inward-facing conformations that expose a centrally located substrate-binding site to the outside or inside of the cell. The structural understanding of this mechanism has been greatly advanced by X-ray crystal structures of prokaryotic *SLC6* homologs captured in principle conformational states of the transport cycle (Penmatsa and Gouaux, 2014).

Elucidating how exogenous ligands bind in SERT and interfere with its conformational behavior is important for understanding the molecular mechanisms of therapeutic drugs such as antidepressants, as well as drugs of abuse. Homology models of SERT have greatly advanced the molecular understanding of inhibitor binding in SERT (Loland, 2015). In contrast, it is poorly understood how drugs affect the overall conformational behavior of SERT. Current insight into mammalian *SLC6* transporter conformations stabilized by drugs is mainly based on biochemical approaches, such as cysteine accessibility or protease and alkylation protection analyses (Zhang and Rudnick, 2006; Jacobs et al., 2007; Tavoulari et al., 2009; Koldso et al., 2013; Gaffaney et al., 2014) that do not offer direct experimental information on specific intraprotein motions occurring during drug binding. Studies of protein dynamics in purified bacterial *SLC6* homologs using Förster resonance energy transfer and electron paramagnetic resonance spectroscopy techniques have identified specific motions associated with alternating access (Kazmier et al., 2014; Kohut et al., 2014);

This work was supported by the Carlsberg Foundation, Lundbeck Foundation, Novo Nordisk Foundation, Hørslev Foundation, and Aase and Ejner Danielsen Foundation.
dx.doi.org/10.1124/mol.115.099911.
[S] This article has supplemental material available at molpharm.aspetjournals.org.

ABBREVIATIONS: cpm, counts per minute; EL, extracellular loop; hSERT, human serotonin transporter; 5-HT, 5-hydroxytryptamine, serotonin; LeuT, leucine transporter; MTS, methanethiosulfonate; SERT, serotonin transporter; TAMRA, 2-([5(6)-tetramethylrhodamine]carboxylamino)ethyl; TEVC, two-electrode voltage clamp; TM, transmembrane; VCF, voltage-clamp fluorometry; WT, wild-type.

however, these techniques have not been available to study mammalian transporters. Voltage-clamp fluorometry (VCF) is a technique that provides real-time correlation between conformational and functional states of electrogenic membrane proteins in a native membrane environment (Gandhi and Olcese, 2008). It utilizes the measurement of changes in emission from residues labeled with environmentally sensitive Cys-conjugated fluorophores to track conformational changes occurring in the immediate vicinity of the fluorophore in parallel with the measurement of membrane currents associated with protein function. Although 5-HT transport is electroneutral, SERT is a source of an inward membrane current proposed to result from the transporter occasionally assuming a channel-like conducting state (Mager et al., 1994; Lin et al., 1996; Schicker et al., 2012). Conductance state occupancy is increased during substrate translocation, whereas inhibitors completely block the state. Thus, the SERT current is excellently suited for monitoring functional states, thereby making the transporter amenable for VCF studies (Li and Lester, 2002).

In the present study, we searched for positions in extracellular regions of SERT at which the fluorophore 2-([5(6)-tetramethylrhodamine]carboxylamino)ethyl (TAMRA) can report conformational changes. We identify four positions that display activity-dependent changes in TAMRA fluorescence and employ these in VCF experiments to monitor and compare conformational changes during transport and inhibition by antidepressants and cocaine. We find that conformational changes occurring upon ligand binding are similar among different types of inhibitors but are different in nature compared with substrate-induced conformational changes.

Materials and Methods

Chemicals were from Sigma-Aldrich (St. Louis, MO), unless otherwise stated. Dulbecco's modified Eagle's medium, fetal bovine serum, trypsin, and penicillin-streptomycin were from Invitrogen (Carlsbad, CA). DNA-modifying enzymes were from New England Biolabs (Ipswich, MA). Cell culture dishes were from Sarstedt AG & Co. (Nümbrecht, Germany), and 96-well plates were from Nunc (Roskilde, Denmark). [^{3}H]5-HT (27–28 Ci/mmol) and the MicroScint-20 scintillation mixture were from PerkinElmer Life Sciences (Waltham, MA). Fluoxetine and escitalopram were kindly provided by H. Lundbeck A/S (Valby, Denmark). 2-([5(6)-Tetramethyl-rhodamine]carboxylamino)ethyl methanethiosulfonate (MTS-TAMRA) was from Biotium (Hayward, CA).

Molecular Biology. The plasmid vector pcDNA3.1 containing human SERT (hSERT) cDNA was used for expression in mammalian cells (Kristensen et al., 2004). Generation of hSERT point mutants was performed by site-directed mutagenesis using the QuickChange mutagenesis kit (Stratagene, La Jolla, CA). The mutations were verified by DNA sequencing of the entire gene (GATC Biotech, Constance, Germany). For confocal imaging of cell-surface expression patterns, hSERT mutants were fused in the *N*-terminal with the GFP^2 variant of enhanced green fluorescent protein (Perkin Elmer, Inc., Dreieich, Germany) as previously described (Sørensen et al., 2012). For the preparation of high-quality capped mRNA by in vitro transcription, the coding domain sequence of hSERT and mutants was subcloned from pcDNA3.1-hSERT into the enhanced *Xenopus* expression vector pGEM-HE (Liman et al., 1992), thereby placing the hSERT cDNA sequence in between 5′- and 3′-untranslated sequences from a *Xenopus laevis* β-globin gene, which has been found to increase translational activity. For use as a template for in vitro transcription of hSERT mRNA, pGEM-HE-hSERT plasmid DNA was linearized with NotI restriction enzyme and purified by phenol/chloroform extraction. Capped mRNA was transcribed as described previously (Poulsen et al., 2013).

Mammalian Cell Culturing and Expression. COS7 cells (American Type Culture Collection, Manassas, VA) were cultured in growth medium (Dulbecco's modified Eagle's medium supplemented with 10% v/v fetal bovine serum, 100 units/ml penicillin, and 100 μg/ml streptomycin) at 37°C in a humidified 5% CO_2 environment. For the expression of wild-type (WT) and mutant hSERT, COS7 cells were transfected using the TransIT DNA transfection reagent (Mirus, Madison, WI) as described previously (Sørensen et al., 2014).

Confocal Imaging. A Leica SP2 confocal microscope equipped with an argon laser, a helium/neon laser, and 63× 1.2 Na HCX PL APO water-corrected objective was used. COS7 cells were replated in 12-well glass bottom plates (MatTek Corporation, Ashland, MA) 24–48 hours after transfection and incubated for 2 hours to adhere. Thirty minutes prior to imaging, cells were stained with CellMask Deep Red plasma membrane stain (Molecular Probes, Inc., Eugene, OR) following instructions provided by the manufacturer. GFP^2-tagged hSERT was visualized using 488 laser lines at 25–35% input power as excitation sources and measurement of emission was in the 500–560 nm spectrum ranges. The cell membrane stain was visualized using the 633-nm helium/neon laser line at 25–35% input power, and the collection of emission was in the –700 nm spectrum range. Overlay images were produced with Leica LAS AF Lite software (Leica Microsystems GmbH, Wetzlar, Germany).

Xenopus Laevis Oocyte Expression. Defoliated stage V–VI oocytes from *Xenopus laevis* were prepared as described previously (Poulsen et al., 2013) and injected with 15-ng mRNA. The care and use of *Xenopus laevis* was in strict adherence to a protocol (license 2014−15−0201−00031) approved by the Danish Veterinary and Food Administration. Injected oocytes were incubated at 18°C in standard Barth's medium containing (in millimolar) 88 NaCl, 1 KCl, 0.41 $CaCl_2$, 2.4 $NaHCO_3$, 0.33 $Ca(NO_3)_2$, 0.82 $MgSO_4$, and 5 Tris (pH 7.4), supplemented with 50 μg/ml gentamicin, and used for current and fluorescence measurements 4–12 days after injection. On the day of the VCF experiments, oocytes were labeled in Barth's medium containing 400 μM MTS-TAMRA for 5 minutes and stored in the dark for up to 2 hours before measurements were performed.

[^{3}H]5-HT Transport Measurements. For the characterization of WT and mutant hSERT transport kinetics, uptake assays were performed in COS7 cells as described previously (Kristensen et al., 2004; Andersen et al., 2009; Sørensen et al., 2012). Briefly, 40–48 hours after transfection, cells were washed twice with 300 μl of phosphate buffered saline containing 0.1 mM $CaCl_2$ and 0.5 mM $MgCl_2$ (PBSCM) and allowed to pre-equilibrate at 20°C for 20–30 minutes in 50 μl of PBSCM per well. For the determination of K_m and V_{max}, saturation uptake experiments were performed. In each experiment, sets of triplicate wells were incubated with eight increasing concentrations of [^{3}H]5-HT diluted 1:25 with an unlabeled substrate at 20°C for 5 minutes, after which uptake was terminated by rapid triple washing of wells with 250 μl of PBSCM. The amount of accumulated radioligand per well was determined by solubilizing cells in 50 μl of scintillation solution (MicroScint20; PerkinElmer), followed by counting of well radioactivity in a Packard TopCounter (PerkinElmer Life Sciences). For cells transfected with WT hSERT, total maximum uptake of [^{3}H]5-HT typically ranged between 1000 and 3000 counts per minute (cpm) per well. Nonspecific uptake was determined by assaying triplicate wells with nontransfected cells in parallel, which typically accumulated between 100 and 500 cpm per well. Specific uptake was calculated by subtracting nonspecific uptake from total uptake. In all experiments, the uptake level was no more than 10% that of total added [^{3}H]5-HT substrate. For each experiment, the K_m and V_{max} value was determined by plotting the mean uptake rate (cpm per minute per well) from triplicate wells as a function of 5-HT concentration and fitted to the Michaelis-Menten equation (see Fig. 1 legend) to obtain the K_m and V_{max} for the given experiment. For each hSERT construct, at least four independent saturation uptake experiments were performed on different days with

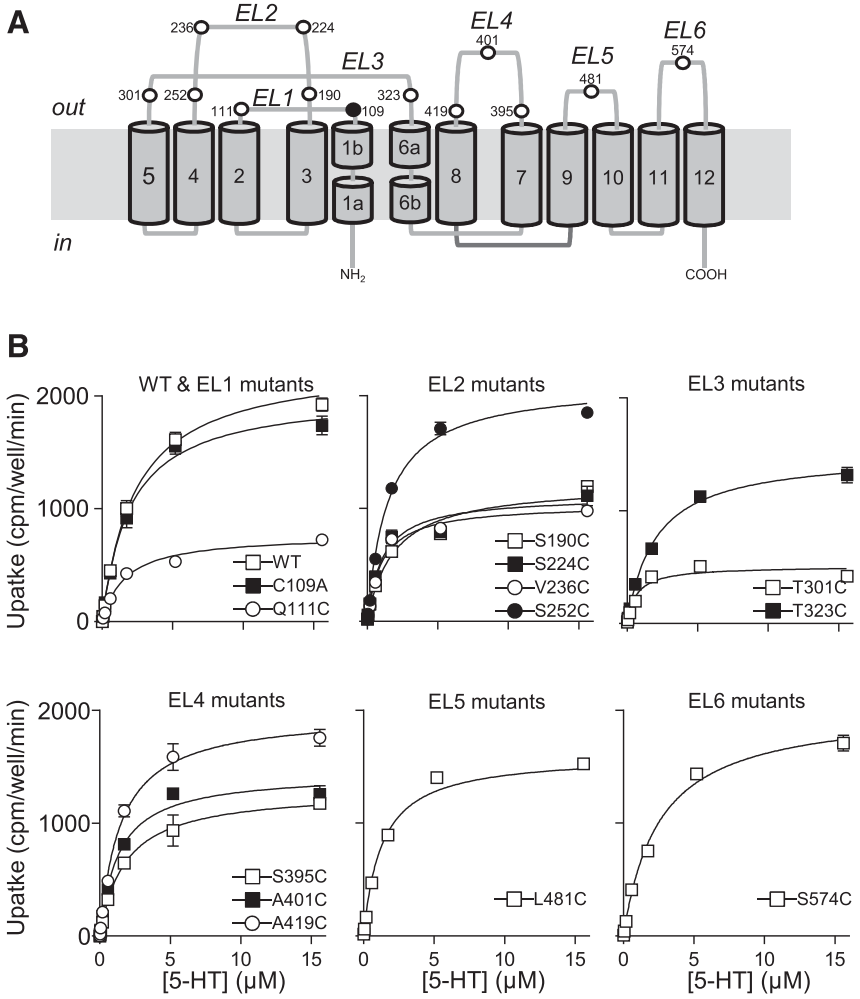

Fig. 1. Location of Cys mutations in hSERT. (A) Overview of the membrane topology of hSERT. Positions in the TM and EL regions where Cys residues were introduced by mutagenesis are shown as white spheres. Endogenous Cys residue 109 is shown as a black sphere. (B) Representative Michaelis-Menten saturation curves describing the relation between substrate uptake rate and substrate concentration in COS7 cells expressing WT and mutant hSERT. Cells were grown in 96-well culture plates and incubated with increasing concentrations of [^{3}H]5-HT for 5 minutes at room temperature, followed by rapid washing of wells and determination of accumulated radioactivity (cpm) in each well by scintillation counting (*Materials and Methods*). Transport rates were calculated as cpm/well per minute following the subtraction of unspecific uptake determined in parallel from wells containing nontransfected cells. Data points represent the mean ± S.E.M. of the uptake rate determined from triplicate wells. K_m and V_{max} were derived by nonlinear regression fitting to the Michaelis-Menten equation $V = V_{max} \times (5\text{-HT})/[K_m + (5\text{-HT})]$, where V is the uptake rate at a given concentration of 5-HT, V_{max} is the maximal uptake rate, and K_m is the Michaelis-Menten constant of 5-HT transport. For each hSERT mutant and for WT hSERT, K_m and V_{max} were determined from at least four independent saturation curves, as summarized in Table 1.

different batches of transfected cells to determine K_m and V_{max}. For the determination of the inhibitor K_i, uptake inhibition experiments were performed. In each experiment, sets of triplicate wells were preincubated with seven increasing concentrations of the inhibitor for 30 minutes before addition of 50 nM [^{3}H]5-HT. Uptake was allowed to proceed for 5 minutes at 20°C, after which uptake was terminated by rapid triple washing of wells with 250 μl of PBSCM before the amount of accumulated radioligand per well was determined as in the saturation uptake experiments. Nonspecific uptake was determined by assaying triplicate wells with nontransfected cells in parallel. Specific uptake was calculated by subtracting nonspecific uptake from total uptake and normalized to the specific uptake from a set of triplicate wells incubated in the absence of the inhibitor. For each experiment, the IC_{50} value was determined by plotting the mean of the normalized uptake from the triplicate wells as a function of inhibitor concentration and fitted to a nonlinear one-site competition curve (see Supplemental Fig. 1) to obtain the IC_{50} for the given experiment. IC_{50} was converted to K_i using the Cheng-Prusoff equation (Cheng and Prusoff, 1973) (see Fig. 3). For each hSERT construct, at least four independent uptake inhibition experiments were performed on different days with different batches of transfected cells. For the determination of the effect of covalent modification with TAMRA on the function and pharmacology of WT and mutant hSERT expressed in COS7 cells, cultured cells grown in 96-well plates were treated with 400 μM MTS-TAMRA (in PBSCM) for 5 minutes, followed by double washing of wells with 250 μl of PBSCM immediately before use in saturation uptake or inhibition experiments (see also Fig. 3 legend).

For the determination of [^{3}H]5-HT transport activity in oocytes expressing hSERT, oocytes were incubated in 160 μl of PBSCM containing 50 nM [^{3}H]5-HT for 30 minutes in 96-well plates, followed by five washes in PBSCM. One molar NaOH was added to dissolve the oocytes, and 5 μl of the solution was transferred to new white 96-well plates. The amount of accumulated radioligand per well was determined by adding 300 μl of scintillation solution, followed by counting of well radioactivity in a Packard TopCounter. For oocytes injected with WT hSERT, total uptake of [^{3}H]5-HT typically ranged between 4000 and 6000 cpm per oocyte. Per experiment, six uninjected oocytes were used as a control and the mean accumulated radioactivity (between 100 to 200 cpm) of these were subtracted to obtain specific uptake. For uptake saturation experiments, a batch of oocytes from a single frog was carefully selected for similar size, development stage, and general appearance and injected with 20 ng hSERT mRNA. Following 6 days of incubation, pools of eight oocytes were incubated for 30 minutes in 24-well plates in 500 μl of PBSCM containing increasing concentrations of [^{3}H]5-HT diluted 1:20 with unlabeled substrate at 20°C for 30 minutes, after which uptake was terminated by rapid washing of each individual oocyte by repeated transferring into 10 ml of PBSCM. The amount of accumulated radioligand per oocyte was determined by placing the oocyte in a 6-ml scintillation vial and solubilizing the oocyte by the addition of 500 μl of 1 M NaOH and incubating for 5 minutes before the addition of 3 ml of scintillation solution (MicroScint20; PerkinElmer), followed by counting of radioactivity in a Tri-Carb liquid scintillation counter (Packard Instrument Co.). For each 5-HT concentration, the amount of nonspecific uptake in six oocytes was determined by assaying noninjected oocytes from the same batch as the

hSERT-injected oocytes in parallel. Specific uptake in each oocyte was calculated by subtracting the mean nonspecific uptake. In all experiments, the total amount of accumulated 5-HT in any oocyte was no more than 5% of the total added [^{3}H]5-HT substrate. The K_m and V_{max} value was determined by plotting the mean uptake rate (cpm per second per oocyte) as a function of 5-HT concentration and fitted to the Michaelis-Menten equation (see Fig. 1 legend).

Voltage Clamp Fluorometry Recordings. Measurements were performed in a perfusion chamber that was mounted on the stage of an inverted epifluorescence microscope (Diaphot 300; Nikon Instruments Europe BV, Amsterdam, The Netherlands) equipped with a 20× air objective. A 100-W xenon lamp, coupled with a rapid monochromator (DeltaRAM X; Photon Technologies International, Surbiton, Surrey, UK), was used to select an excitation wavelength of 535 nm. Emission was filtered using the G-1B filter set from Nikon, with the excitation filter removed (565-nm dichromatic mirror and 590-nm longpass emission filter). Emission intensity was measured with a D104 photomultiplier tube photometer system (Photon Technologies International), with the photomultiplier tube set at 500–700 V. The membrane current and voltage were measured under a two-electrode voltage clamp (TEVC) as described previously (Poulsen et al., 2013). Oocytes were perfused continuously at 5 ml/min with Ca^{2+}-free Frog Ringer buffer (in millimolar: 115 NaCl, 2.5 KCl, 1.8 $MgCl_2$, 1.8 $BaCl_2$, and 10 HEPES, pH 7.4 with NaOH). Electrodes were filled with 3 M KCl and had a resistance of <2 MΩ. The bath clamp electrodes were connected directly to the bath. The holding potential was maintained at −80 mV unless specified otherwise. Fluorescence and current signals were digitized using an analog-digital converter (DigiData 1322, Molecular Devices, Sunnyvale, CA) interfaced with a personal computer running Clampex 10 software (Molecular Devices). Current and fluorescence signals were digitally low-pass filtered off-line at 5 and 1 Hz, respectively. All recordings were performed at room temperature (20–22°C).

Data and Statistical Analysis. Data and statistical analyses were performed using pClamp 10 (Molecular Devices) or Prism 6.0 (GraphPad Inc., San Diego, CA) software. Analysis of 5-HT transport kinetics was performed as described previously (Sørensen et al., 2012). The molecular graphics program PyMOL was used for structural alignments and visualization (http://www.pymol.org). Unless otherwise noted, all statistical comparisons were performed using analysis of variance.

Results

Introduction of Cys Residues in Transmembrane and Extracellular Loop Regions of hSERT. Site-directed fluorophore labeling of introduced Cys residues requires removal of all endogenous Cys residues that are reactive to extracellular applied thiol-reactive fluorophores. Previous work has shown that hSERT contains three endogenous extracellular Cys residues located in the top of transmembrane (TM) 1b and extracellular loop (EL) 2. C200 and C209 in EL2 are linked by an endogenous disulfide bond and are unreactive to MTS or maleimide-based reagents, whereas C109 in TM1b is reactive (Chen et al., 1997, 1998; Li and Lester, 2002). To enable site-specific conjugation of fluorophore to Cys residues introduced by site-directed mutagenesis, we replaced C109 by Ala. This C109A mutation does not alter hSERT transport or electrophysiological function and removes extracellular thiol reactivity of hSERT (Chen et al., 1997; Li and Lester, 2002). The resulting hSERT-C109A was used as a background for the introduction of all subsequent single Cys mutations in TM and EL regions (Fig. 1A). For the selection of extracellular positions in hSERT to insert Cys, we used a previously published homology model of hSERT based on the prototypical bacterial *SLC6* homolog, the leucine transporter (LeuT) (Andersen et al., 2010). One to four residues were mutated to Cys in each EL region or close to the N- or C-terminal ends of the adjacent TM regions that are connected by the respective loops (Fig. 1A). These positions were chosen because 1) they were predicted to be exposed to the extracellular environment and 2) they have not been reported to be involved in substrate transport or inhibitor binding and/or to tolerate replacement by Cys. We expressed the Cys mutants along with WT hSERT and hSERT-C109A in COS7 cells and performed measurements of [^{3}H]5-HT uptake to determine the potential impact of the mutations on hSERT transport function. The results from saturation uptake experiments in COS7 cells showed K_m values and maximal transport velocities (V_{max}) for all mutants to be similar to WT hSERT and the parent C109A mutant (Fig. 1B; Table 1), showing that all mutants have unchanged or grossly intact transport function in COS7 cells. As a first test of the ability of the mutants to functionally express in *Xenopus laevis* oocytes (the amphibian expression system needed for VCF measurements), we prepared cRNA for mutant and WT hSERT and injected this into *Xenopus laevis* oocytes and measured uptake of [^{3}H]5-HT at a single concentration of 50 nM [^{3}H]5-HT (*Materials and Methods*) (Table 1). Overall, all mutants displayed specific uptake in oocytes following 4–6 days of incubation, thereby demonstrating capability of the entire mutant library to be heterologously expressed with intact transport function in these amphibian cells and thus be potentially useful for VCF experiments. The transport activity for S190C, S252C, T323C, S395C, A419C, L481C, and S574C were within an ~50% range of the parent hSERT-C109A and WT hSERT, whereas the remaining mutants Q111C, S224C, V236C, T301C, and A410C displayed transport activities that were substantially lower (5–14% of the uptake rate in WT hSERT) (Table 1). It is technically difficult

TABLE 1
Effect of Cys mutations on hSERT transport in COS7 cells and *Xenopus* oocytes

hSERT Mutation	K_m[a]	n[b]	COS7 Cell		Xenopus Oocytes	
			V_{max}[a,c]	n[b]	5-HT Uptake[d]	n[e]
	μM		*% of WT*		*% of WT*	
WT	1.31 ± 0.16	15	100	15	100	31
C109A	1.78 ± 0.16	15	93 ± 4	15	84 ± 6	21
C109A-Q111C	1.32 ± 0.29	7	34 ± 3*	7	9 ± 2*	11
C109A-S190C	0.82 ± 0.14	5	69 ± 5*	5	81 ± 5	20
C109A-S224C	1.36 ± 0.35	4	64 ± 7*	4	5 ± 1*	3
C109A-V236C	1.08 ± 0.17	6	43 ± 2*	6	14 ± 5*	5
C109A-S252C	1.37 ± 0.08	6	97 ± 5	6	33 ± 7*	16
C109A-T301C	1.42 ± 0.23	8	44 ± 4*	8	11 ± 2*	6
C109A-T323C	1.56 ± 0.14	7	79 ± 10	4	52 ± 4*	22
C109A-S395C	1.44 ± 0.32	4	75 ± 15	4	41 ± 7*	9
C109A-A401C	1.45 ± 0.09	5	81 ± 9	5	14 ± 2*	7
C109A-A419C	1.74 ± 0.13	4	116 ± 17	4	111 ± 9	16
C109A-L481C	1.38 ± 0.09	4	78 ± 4	4	82 ± 9	8
C109A-S574C	1.93 ± 0.23	4	94 ± 9	4	27 ± 3*	13

[a]Values are mean ± S.E.M.
[b]Number of individual uptake saturation experiments performed as described in the legend to Fig. 1 and in *Materials and Methods*.
[c]Expressed as percentage of WT determined in parallel. For WT, V_{max} (mean ± S.E.M.) was 109 ± 12 fmol/min per well (n = 15).
[d]Values are mean ± S.E.M. of the uptake measured at a concentration of 50 nM [^{3}H]5-HT and expressed as the percentage of uptake in WT hSERT-expressing oocytes assayed in parallel. For WT, the 5-HT uptake (mean ± S.E.M.) is 1.58 ± 0.11 pmol/min per oocyte (n = 37).
[e]Number of individual oocytes.
*$P < 0.05$, significantly different from WT (analysis of variance).

to perform comparative saturation uptake determinations of 5-HT uptake kinetics of WT and mutant hSERT expressed in *Xenopus laevis* oocytes as this expression system can display a large variation in transporter expression levels between individual oocytes. This is because oocytes as individual cells have inherent differences in expression capacity and furthermore need to be individually microinjected with nanoliter volumes of mRNA solutions, which may further induce variation in expression levels. However, previous work examining the uptake function of heterologously expressed SERT in *Xenopus laevis* oocytes has shown that the obtained Michaelis-Menten constants (K_m) are very similar between these expression systems, thus strongly suggesting that the molecular function of heterologously expressed SERT is grossly the same in these expression hosts. To further ensure that our analysis in COS7 cells of the potential effects of Cys-mutation on hSERT transport function (Fig. 1; Table 1) is a good proxy for the uptake kinetics in oocytes, we performed saturation uptake on WT hSERT expressed in oocytes (*Materials and Methods*) and compared the resulting concentration-uptake relationship with that observed in COS7 cells (Supplemental Fig. 1). The results showed that the saturation curves were similar and yielded a similar K_m for 5-HT uptake and confirmed the previous determination of K_m in *Xenopus laevis* oocytes (Quick, 2003). Thus, we found that it was not necessary to perform a saturation uptake analysis of the Cys mutant library in *Xenopus laevis* oocytes.

Identification of Cys Mutants Displaying Activity-Dependent Fluorescence Changes. To identify Cys mutants useful for VCF experiments, we initially expressed the mutants, along with WT hSERT and C109A in oocytes, and screened these for activity-dependent changes in membrane fluorescence following labeling with MTS-TAMRA (*Materials and Methods*) under TEVC, thereby enabling simultaneous recording of fluorescence with a SERT-mediated membrane current. Following incubation with MTS-TAMRA, time-resolved measurements of the oocyte membrane current and fluorescence were recorded during application of 10 μM 5-HT to stimulate transport activity and associated conformational changes in hSERT. The standard recording protocol and representative fluorescence traces are shown in Fig. 2. To exclude that background fluorescence mediates any 5-HT fluorescence changes per se, recordings of membrane fluorescence were performed on uninjected oocytes in parallel (Fig. 2A). Neither uninjected oocytes nor oocytes expressing hSERT-C109A showed changes in TAMRA fluorescence (ΔF) in response to 5-HT that were above the general signal-to-noise detection limit of our VCF setup (Fig. 2A). Three mutants (T323C, A419C, and L481C) showed pronounced and robust fluorescent and current responses (Fig. 2). In addition, WT hSERT, which is labeled at the endogenous Cys109, displayed robust fluorescence responses, in accordance with previous findings for rat SERT (Li and Lester, 2002). Specifically, for oocytes injected with WT hSERT and T323C, A419C, and L481C mutants, reversible decreases in membrane fluorescence were observed upon application of 5-HT, which correlated with an increase in the hSERT-mediated current (Fig. 2A). In general, in oocytes expressing these mutants, the amplitude of the associated 5-HT current was in the range of 10–100 nA (Fig. 2C), which is within the typical range of previously reported TEVC characterizations of hSERT expressed in oocytes (Li and Lester, 2002). The parallel decrease in TAMRA fluorescence was in the order of 0.5–3.8% of the total membrane fluorescence (Fig. 2B), with a time course that mirrored the time course of the 5-HT–evoked current response. Thus, these 5-HT–evoked changes in TAMRA fluorescence (ΔF) show that 109, 323, 419, and 481 positions in hSERT can be used to report molecular rearrangements associated with transport function following labeling with TAMRA. Robust ΔF in response to 5-HT application was also detected in oocytes expressing Q111C, T301C, and A401C (Fig. 2B). However, for the Q111C and A401C mutants, no or very small 5-HT–evoked current responses were associated with the observed ΔF (Fig. 2C), suggesting that Cys mutation or subsequent TAMRA labeling has perturbed the electrophysiological properties of the transporter. Oocytes expressing T301C did display small 5-HT–evoked current responses, but in the form of decreases in the membrane current (Fig. 2C). The opposite direction of the 5-HT–evoked current response at T301C compared with WT hSERT suggests that TAMRA conjugation at this position substantially changes the electrophysiological properties of hSERT. Thus, although Q111C, T301C, and A401C displayed promising properties in terms of robust fluorescence changes associated with 5-HT application, the substantial changes in electrophysiological properties induced by Cys mutation and/or TAMRA labeling as well as their generally lowering of 5-HT uptake activity when expressed in *Xenopus* oocytes (Table 1) led us to consider these mutants as poor candidates for use in further VCF measurements and they were therefore not pursued further. The remaining mutants (S190C, S224C, V252C, V263C, and S395C) showed no fluorescence changes (Fig. 2B) and were therefore not pursued further.

Characterization of T323C, A419C, and L481C for TAMRA-Conjugated Effects on hSERT Function and Pharmacology. Following the identification of the hSERT mutants T323C, A419C, and L481C as those displaying robust activity-dependent ΔF, we further characterized these mutants and WT hSERT, with respect to electrophysiological properties, transport function, and inhibitor pharmacology after TAMRA labeling to determine whether Cys introduction and covalent modification with the fluorophore perturbed these properties. The initial characterization of the transport function of T323C, A419C, and L481C showed grossly intact K_m and V_{max} of the mutants compared with WT hSERT (Fig. 1; Table 1). Analysis of the cell-surface expression of these three Cys mutants in COS7 cells using confocal imaging of GFP[2]-fused transporters (*Materials and Methods*) showed that T323C, A419C, and L481C were expressed in the cell surface membrane similar to WT hSERT (Fig. 3A). These results further suggest that introduction of T323C, A419C, or L481C in the C109A background does not change the ability of hSERT to express with intact functional properties. To investigate if covalent modification with TAMRA of the endogenous Cys109 or Cys introduced at the 323, 419, and 481 positions perturbed transport function, we determined K_m and V_{max} for [^{3}H]5-HT transport of WT hSERT and T323C, A419C, and L481C expressed in COS7 cells following treatment with TAMRA (Fig. 3B; Supplemental Table 1). The results showed that covalent modification with TAMRA of these residues had no significant effect on K_m but decreased V_{max} significantly by 63, 36, and 21% at T323C, A419C, and L481C, respectively (Supplemental Table 1). However, we

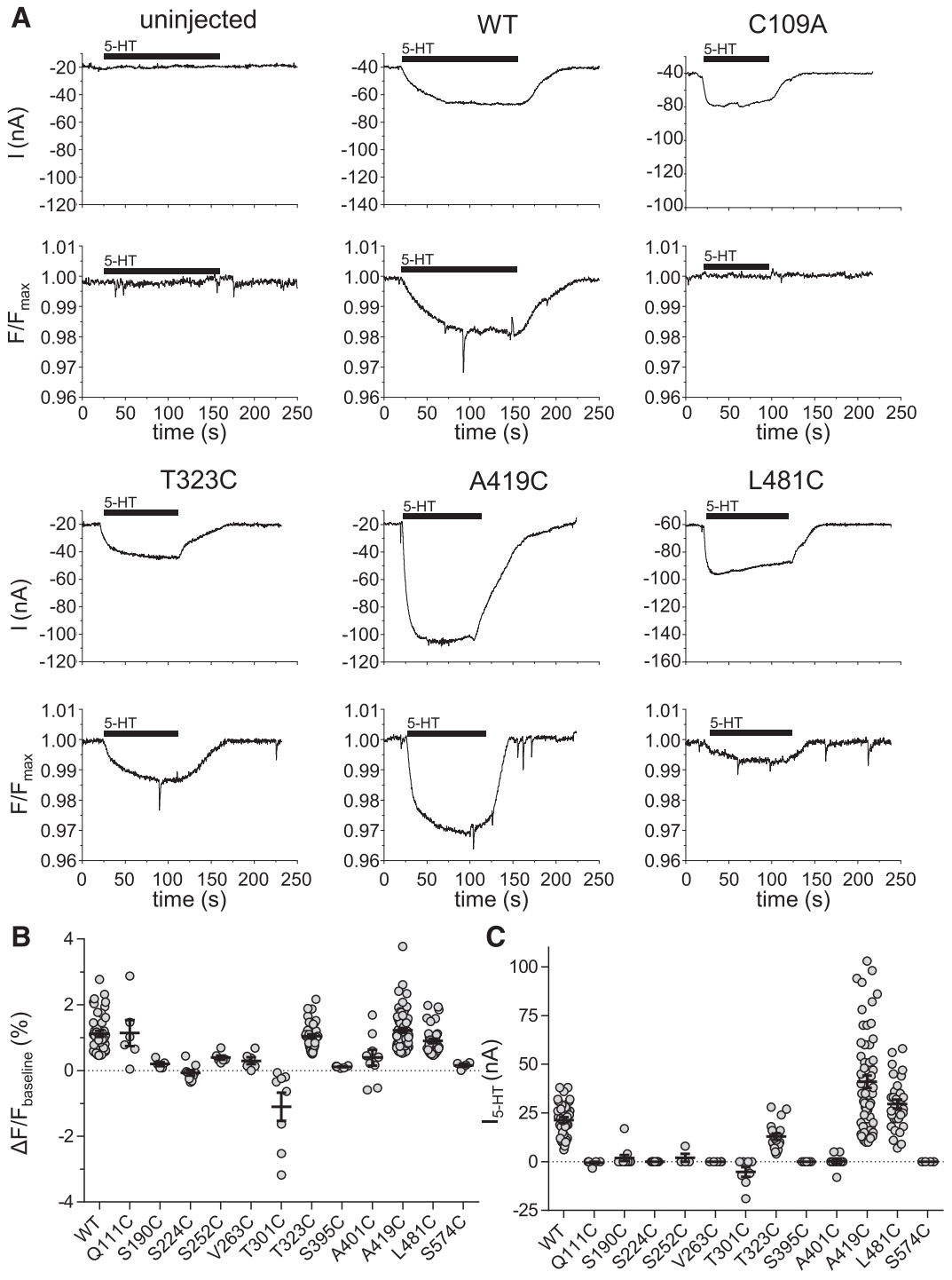

Fig. 2. Fluorescent measurements identify Cys mutants reporting conformational changes in hSERT related to 5-HT transport. (A) Representative recording traces of parallel fluorescence and current measurements from oocytes expressing WT hSERT, C109A, C109A-T323C, and C109A-A419C during application of 10 μM 5-HT (black line). Oocytes were held at −80 mV during the experiments. Upper traces show membrane currents (I), and lower traces show the corresponding membrane fluorescence signal (F/F_{max}) normalized to the fluorescence intensity obtained immediately after start of excitation. (B and C) Summary of fluorescence changes (ΔF) and current ($I_{5\text{-HT}}$) evoked by application of 5-HT. Shown are scatter plots of ΔF (B) and $I_{5\text{-HT}}$ (C) from individual oocytes injected with WT hSERT and Cys mutants. ΔF is calculated as the percentage difference between baseline fluorescence and steady-state fluorescence during 5-HT application. Black bars represent ΔF (mean ± S.E.M.): WT, 1.11 ± 0.09% (43 oocytes); Q111C, 1.14 ± 0.40% (six oocytes); S190C, 0.19 ± 0.05% (five oocytes); S224C, −0.07 ± 0.08% (nine oocytes); S252C, 0.39 ± 0.07% (six oocytes); V263C, 0.29 ± 0.10% (six oocytes); T301C, −1.10 ± 0.42% (eight oocytes); T323C, 1.04 ± 0.06% (41 oocytes); S395C, 0.11 ± 0.01% (six oocytes); A401C, 0.39 ± 0.24% (nine oocytes); A419C, 1.22 ± 0.07% (65 oocytes); L481C, 0.90 ± 0.06% (37 oocytes); S574C, 0.16 ± 0.05% (four oocytes).

considered these effects to be tolerable in relation to the use of the mutants in further VCF experiments. To investigate that the introduced Cys residues and covalent modification by TAMRA did not change the sensitivity of the transporters to inhibitors, we determined the inhibitory potency of the inhibitors escitalopram, fluoxetine, and cocaine at WT hSERT

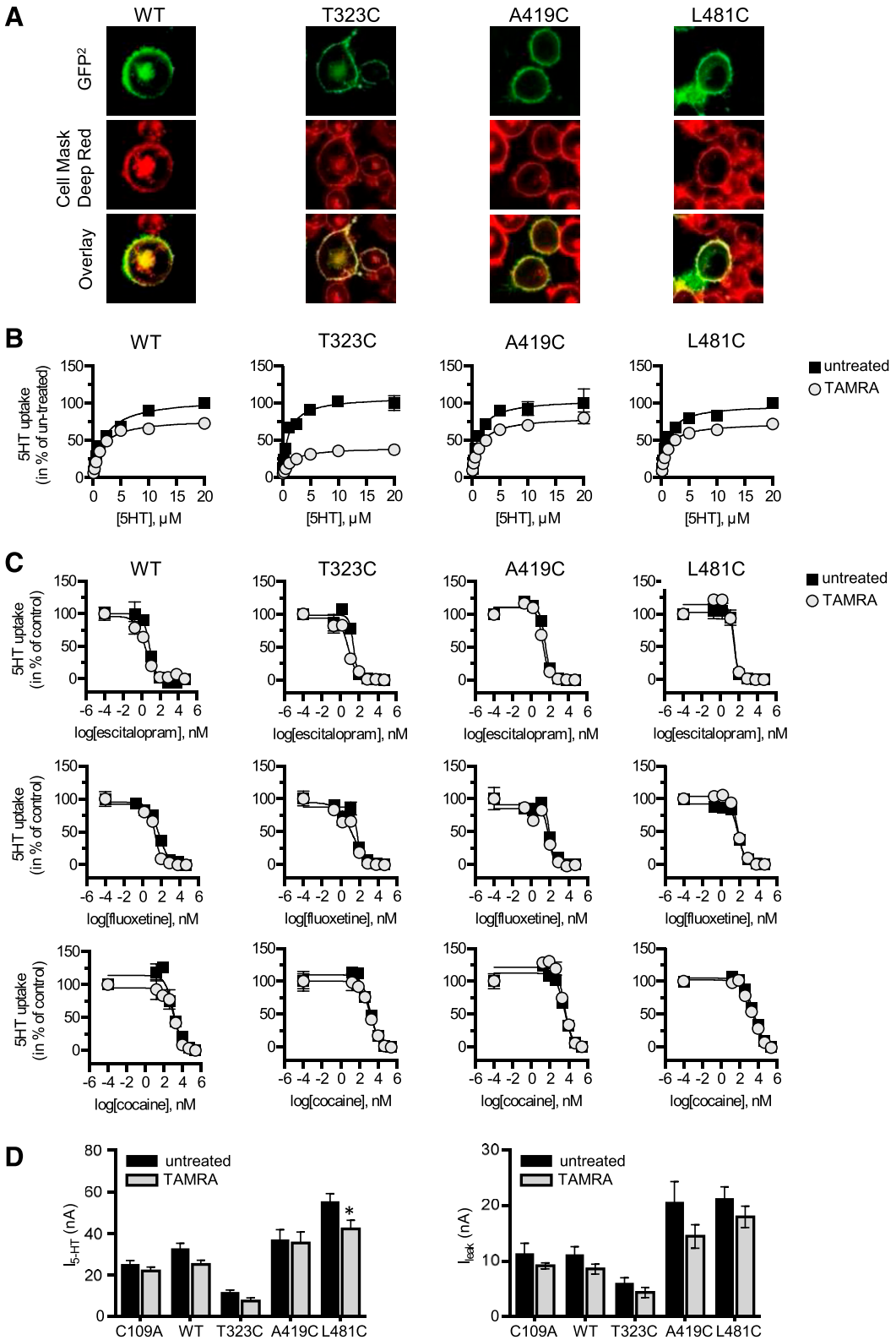

Fig. 3. Effect of Cys mutation and covalent modification with TAMRA on hSERT properties. (A) Confocal imaging of COS7 cells expressing WT and hSERT mutants to visualize distribution of GFP^2-tagged transporter (green; upper panel) and Cell Mask Deep Red stained cell surface membrane (red; middle panel). Colocalization of cell surface membrane stain and GFP^2-tagged transporter is visualized by merging upper and middle images (lower panel), thereby appearing yellow. (B) Effect of covalent modification with TAMRA on transport function. Representative curves from paired saturation uptake experiments with untreated (■) and TAMRA-treated (○) COS7 cells expressing WT hSERT and Cys mutants performed as described in the legend of Fig. 1. (C) Effect of TAMRA treatment on inhibitor pharmacology of WT and mutant hSERT. Representative dose-response curves from paired uptake inhibition experiments with escitalopram (upper), fluoxetine (middle), and cocaine (lower) with untreated (■) and TAMRA-treated (○) COS7 cells expressing WT hSERT and Cys mutants (*Materials and Methods*). Data points represent the mean from triplicate determinations. Error bars are S.E.M. and shown when larger than symbols. The data were plotted versus the log of the molar concentration of the inhibitor and fit to a nonlinear one-site competition curve defined by the

and T323C, A419C, and L481C expressed in COS7 cells in the absence and presence of TAMRA labeling (Fig. 3C). The results showed that Cys substitution and/or covalent modification with TAMRA at these positions did not change the inhibitory potency of these inhibitors (Supplemental Table 2), which is in good agreement with the prediction that amino acid positions 109, 323, 419, and 481 are located well outside of the binding pocket for these inhibitors in hSERT. To determine whether covalent modification by TAMRA at the four reporter positions changed the electrophysiological properties of hSERT, we performed measurements of the constitutive hSERT-mediated leak current and the 5-HT–evoked current (from now on defined as I_{leak} and $I_{5\text{-HT}}$, respectively) on oocyte batches expressing WT hSERT and the Cys mutants, in which half of the oocytes were treated with TAMRA, whereas the other half was left untreated. The results showed that there were no significant changes in the amplitude of I_{leak} and $I_{5\text{-HT}}$ among untreated and TAMRA-treated oocytes for any of the Cys mutants or for WT hSERT, except for a small but significant decrease of $I_{5\text{-HT}}$ for L481C (Fig. 3D). These results suggest that the introduction of Cys residues and covalent modification by TAMRA do not grossly perturb hSERT electrophysiological properties, thereby allowing measurements of I_{leak} and $I_{5\text{-HT}}$ mediated currents to be used as a readout of transporter function for correlation with fluorescence changes as a readout of conformational changes.

Characterization of Fluorescent Changes during Inhibitor Binding. We next performed VCF measurements of the membrane current and TAMRA fluorescence from oocytes expressing WT-hSERT, T323C, A419C, and L481C during application of different SERT inhibitors to investigate potential conformational changes upon inhibitor binding. To this end, three inhibitors were tested: cocaine and the selective serotonin reuptake inhibitors escitalopram and fluoxetine. Our standard recording protocol employed for these experiments is illustrated in Fig. 4A and contains an initial application of a saturating concentration of 5-HT to elicit a ΔF that represents the transition of the transporter population from the outward-facing state to the inward-facing state. The initial 5-HT stimulus is then followed by a wash-out period before a saturating concentration of inhibitor is applied to the oocyte (1 μM cocaine, 10 μM escitalopram, and 30 μM fluoxetine, respectively). We were not able to perform recordings of sequential application of all inhibitors to the same oocyte due to the slow inhibitor unbinding rates, in particular that of escitalopram, which would require long wash-out periods and increase the overall recording time to more than 30 minutes, resulting in unstable current recordings and loss of TAMRA labeling as well as TAMRA photo bleaching. We also performed measurements of membrane fluorescence and current from uninjected oocytes and oocytes expressing the C109A mutant labeled with TAMRA to verify that the inhibitors, when applied in the chosen working concentrations, did not change fluorescence originating from nonspecific labeling of endogenous Cys in the oocyte membranes. For all inhibitors, we did not detect changes in background fluorescence (Fig. 4B). The recordings from oocytes expressing WT hSERT, T323C, A419C, and L481C showed that escitalopram evoked a detectable ΔF at WT hSERT, A419C, and L481C, whereas fluoxetine and cocaine evoked a detectable ΔF at all four constructs (Fig. 4B). The time course of the inhibitor-evoked fluorescence changes was overall well aligned with the time course of the corresponding I_{leak}, indicating that the observed ΔF reflects the conformational transition from the resting apo state to an inhibitor-bound state. However, the amplitude and direction of the fluorescence response varied among the positions. A419C and L481C displayed decreases in fluorescence for all three inhibitors, with ΔF in the range of around -0.25%. These results indicate that hSERT undergoes conformational changes in the regions surrounding Ala419 in EL4 and Leu481 in EL5 during inhibitor binding. In contrast, WT hSERT, which is labeled at Cys109, displayed increases in fluorescence for fluoxetine and escitalopram in the range of 0.5% (Fig. 4B). Cocaine also increased fluorescence from Cys109, but not to a degree that was significantly different from control conditions (uninjected oocytes and C109A) (Fig. 4B), for which none of the ligands produced changes in TAMRA fluorescence that were above the signal-to-noise detection limit of our VCF setup (Fig. 4B).

The amplitude of fluorescence signals was, in general, found to vary substantially among individual oocytes that had been injected, incubated, and labeled in parallel. This is due to inherent differences among oocytes that affect transporter expression level, background, and specific labeling of the protein. Therefore, to enable comparative analysis of the inhibitor-evoked fluorescence responses, we normalized the amplitude of the inhibitor response to the 5-HT response (evoked at the beginning of each recording) for each oocyte (Fig. 5). This allowed us to compare the amplitudes of the responses produced at the four measured positions in hSERT among the inhibitors. The results show that cocaine, fluoxetine, and escitalopram overall evoke a quite similar pattern of fluorescence changes from the four positions (Fig. 5). Thus, as these fluorescent "fingerprints" represent conformational changes at four different positions well dispersed around the hSERT extracellular region, their similarity suggests that binding of all three inhibitors induce similar conformational changes in hSERT around the top of TM1b, TM6, EL4, and EL5, strongly suggesting that the inhibitors stabilize the same conformational state of hSERT. Furthermore, it is apparent that the conformational changes are quite distinct from those evoked by 5-HT, most strikingly at position 109, where the inhibitor-evoked fluorescence changes are opposite in the direction of the change evoked by 5-HT. For all positions, we observed that the inhibitors, in general, evoked much smaller fluorescence changes (10–45%)

equation: % uptake = $100/[1 + 10^{\wedge}([\log IC_{50} - \log (\text{inhibitor})]n_H)]$, where IC_{50} is the concentration of the inhibitor that produces a half-maximal inhibition of uptake and n_H is the Hill slope. IC_{50} values were converted to K_i values using the Cheng-Prusoff equation (Cheng and Prusoff, 1973) $K_i = IC_{50}/(1 + ([L]/K_m)$, where [L] is the concentration of [^{3}H]5-HT and K_m is the Michaelis-Menten constant for transport of 5-HT (Supplemental Table 2; Table 1). (D) Summary of amplitudes of $I_{5\text{-HT}}$ and I_{leak} in oocytes expressing WT and Cys-mutant hSERT with (gray bars) or without (black bars) MTS-TAMRA treatment. Currents were measured as described in Fig. 2. Data represent the mean ± S.E.M. for 12–25 individual oocytes for each condition. *$P < 0.05$; significantly different from untreated.

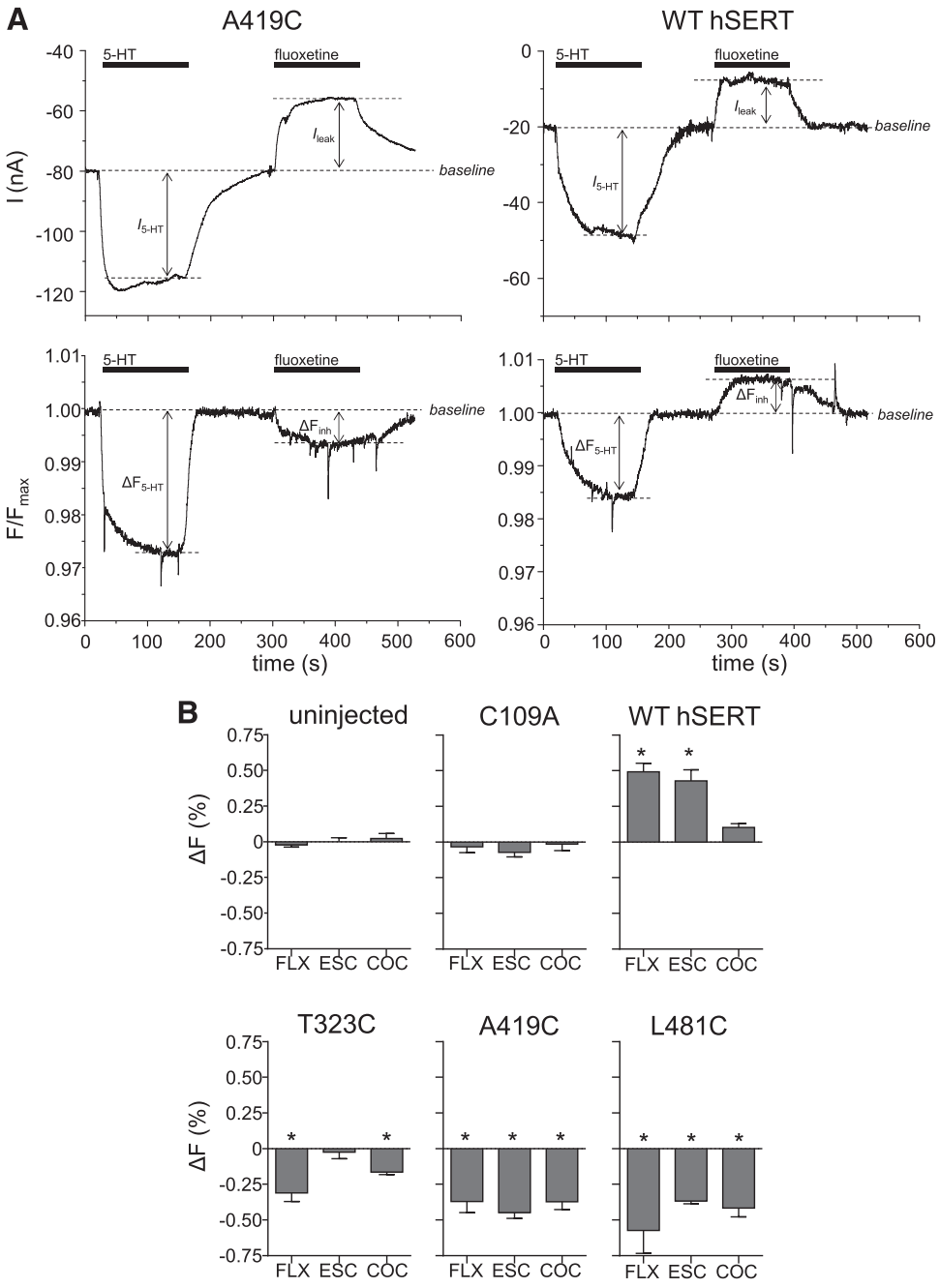

Fig. 4. Inhibitor-induced fluorescence changes in hSERT. (A) Recording traces of parallel measurements of membrane current and fluorescence from representative oocytes expressing TAMRA-labeled A419C and WT hSERT during application of 10 μM 5-HT and 10 μM fluoxetine (black lines). Oocytes were held at −80 mV during the experiments. The top traces show membrane currents (I), and the lower traces show the concomitant membrane fluorescence signal (F/F_{max}) normalized to the fluorescence intensity obtained immediately after the start of excitation. Arrows indicate current responses produced by 5-HT ($I_{5\text{-HT}}$) and inhibitor (I_{leak}) and the corresponding fluorescence responses ($\Delta F_{5\text{-HT}}$ and ΔF_{inh}, respectively). Baseline and steady-state levels of the membrane current and fluorescence are indicated with stippled lines. (B) Summary of ΔF_{inh} for fluoxetine (FLX), escitalopram (ESC), and cocaine (COC) at WT hSERT, C109A, Cys mutants, and uninjected oocytes. Data represent the mean ± S.E.M. for 6–25 individual oocytes for each condition. *$P < 0.05$; significantly different from control (uninjected oocytes).

compared with those evoked by 5-HT. Under the assumption that 5-HT application promotes transition from the apo outward-facing open state of the transporter population to an inward-facing dominated population overall, these results may suggests that the inhibitor-bound conformations are closer to but different from the apo outward-facing open state than to the inward-facing conformation.

Discussion

Crystal structures of bacterial *SLC6* transporter homologs have provided a pivotal starting point for understanding the principal structural transitions underlying transport (Yamashita et al., 2005; Singh et al., 2008; Krishnamurthy and Gouaux, 2012; Malinauskaite et al., 2014). Nevertheless, static structures do not provide information on the dynamic behavior of the transporter protein in a native membrane environment. Molecular dynamics simulations can be used to study transporter dynamics. However, as computational techniques, molecular dynamics simulations rely on experimental validation of proposed mechanisms. An important overall result of the present study is therefore the establishment of VCF procedures for direct monitoring of conformational changes within hSERT. Previous VCF studies on SERT (Li and Lester, 2002) and the related γ-aminobutyric acid transporter GAT1 (Li et al., 2000; Meinild et al., 2009; Meinild and Forster, 2012) have used a single conserved endogenous Cys in TM1. Importantly, our results show several other regions of hSERT to be highly amenable to VCF characterization and identify three additional reporter positions that robustly and reproducibly

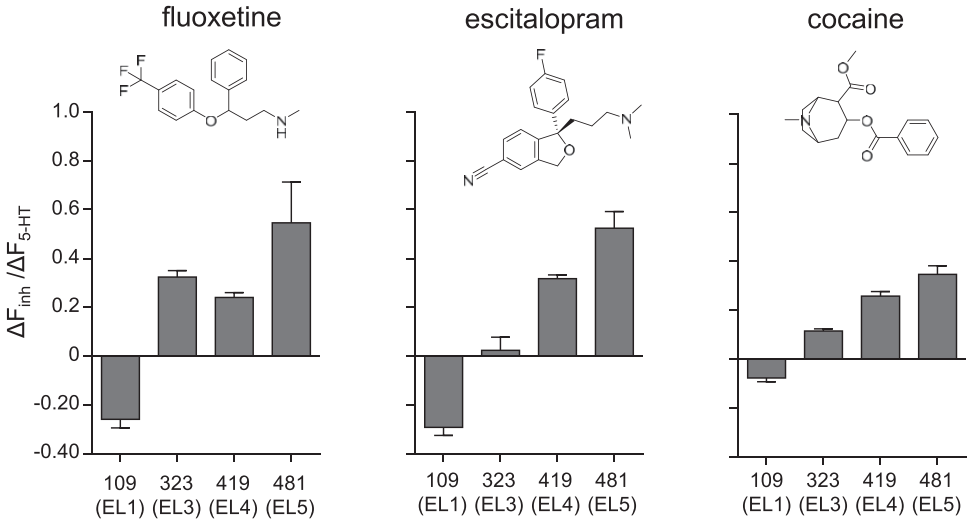

Fig. 5. Comparison of hSERT fluorescence response patterns among inhibitors. Graphical presentation of fluorescence response amplitudes from the four reporter positions in hSERT to fluoxetine (left), escitalopram (middle), and cocaine (right) normalized to the 5-HT response. For each condition, data represent the mean ± S.E.M. for 6–25 recordings of individual oocytes, for which ΔF_{inh} was normalized to a preceding $\Delta F_{5\text{-HT}}$.

can report fluorescence changes without perturbation of function.

The ability to correlate SERT-mediated currents with fluorescence provides novel insight regarding structural movements associated with transport and inhibitor binding. In the absence of the substrate (apo state), Na^+-coupled transporters of the *SLC6* fold are stabilized in the outward-facing open conformation (Zhao et al., 2012; Gaffaney et al., 2014; Kazmier et al., 2014; Malinauskaite et al., 2014; Sandtner et al., 2014). Thus, prior to 5-HT application, the cell-surface population of hSERT is dominated by this apo state, whereas during 5-HT application, the transporter population becomes engaged in transport, adopting all potential conformational states of the alternating access cycle. The ΔF observed upon 5-HT application represents the ensemble conformational changes associated with the shift from outward facing being the dominant state to an equilibrium of all potential conformational states of the transport cycle. However, because the rate-limiting step in the transport cycle is the transition of the substrate-empty transporter from the inward-facing conformation to the outward-facing conformation (Bulling et al., 2012; Schicker et al., 2012; Felts et al., 2014), inward-facing conformations become dominant under saturating substrate conditions. Therefore, in our recording protocol, the conformational changes underlying ΔF evoked by 5-HT application likely represents transition from an outward-facing conformation to an inward-facing conformation of hSERT. For this transition, our data suggest structural rearrangement around Cys109 and Thr323 located in the top of TM1b and TM6a, respectively. These observations fit well with current models of the main outward-to-inward transition of *SLC6* transporters to involve movements within a four-helix bundle composed of TM1–TM2 and TM6–TM7, either through a concerted motion of the entire bundle (Forrest and Rudnick, 2009) or through a set of sequential transitions (Kazmier et al., 2014; LeVine and Weinstein, 2014; Penmatsa and Gouaux, 2014). As the regions containing the Cys109 and Thr323 reporter positions are well conserved between LeuT and hSERT (Fig. 6A), insight into the structural changes that the attached fluorophore may experience during transitions can be provided from a comparison of structures of LeuT in the substrate-free outward- and inward-facing open states (Krishnamurthy and Gouaux, 2012) and the substrate-bound outward-facing occluded state (Yamashita et al., 2005). As shown in Fig. 6B, structural overlay of these structures shows that Ala35 in TM1b and Pro241 in TM6 (corresponding to Cys109 and Thr323 in hSERT, respectively; Fig. 6B) are gradually transposed by 8.1 and 5.8 Å, respectively, from the outward-facing open conformation to the inward-facing conformation. In both these motions, attached fluorophores at Cys109 and Thr323 may become more buried in the transporter structure, potentially leading to increased fluorophore quenching. Assuming that 5-HT stimulation shifts the conformational equilibrium of hSERT from outward facing to inward facing, then the negative ΔF observed for the Cys109 and Thr323 reporter positions likely reflects direct movement of the TM1b and TM6a regions. The reporter positions Ala419 and Leu481 are located at the top of TM8 and TM9, respectively. These TMs are not contained in the core group of helices thought to move during the outward-to-inward transitions, but are instead part of a rigid scaffold proposed to remain static overall during the transport cycle (Penmatsa and Gouaux, 2014). However, the LeuT structure overlays indicate that the residue Gly336 (corresponding to Ala419 in hSERT) may still be displaced by 3.3 Å between the outward- and inward-facing conformations (Fig. 6B). Calculation of the potential spatial arrangement of LeuT in the lipid bilayer using the Orientations of Proteins in Membranes database (http://opm.phar.umich.edu/) (Lomize et al., 2006) predicts Gly336 to be exposed to the extracellular surface of the lipid bilayer. The predicted translation moves this position further toward the membrane. A similar translation of the corresponding region in hSERT may potentially lead to increased quenching of an attached fluorophore by the hydrocarbon interior of the membrane. Met394 (corresponding to Leu481 in hSERT) at the top of TM9 is also located close to the extracellular surface of the lipid bilayer, but is not predicted to change position during state transitions (Fig. 6B). Thus, the fluorescence decrease from the corresponding reporter position in hSERT upon 5-HT application may not be explained from direct movement of the fluorophore relative to the membrane. More likely, this quenching is produced by movements of peripheral elements in the transporter

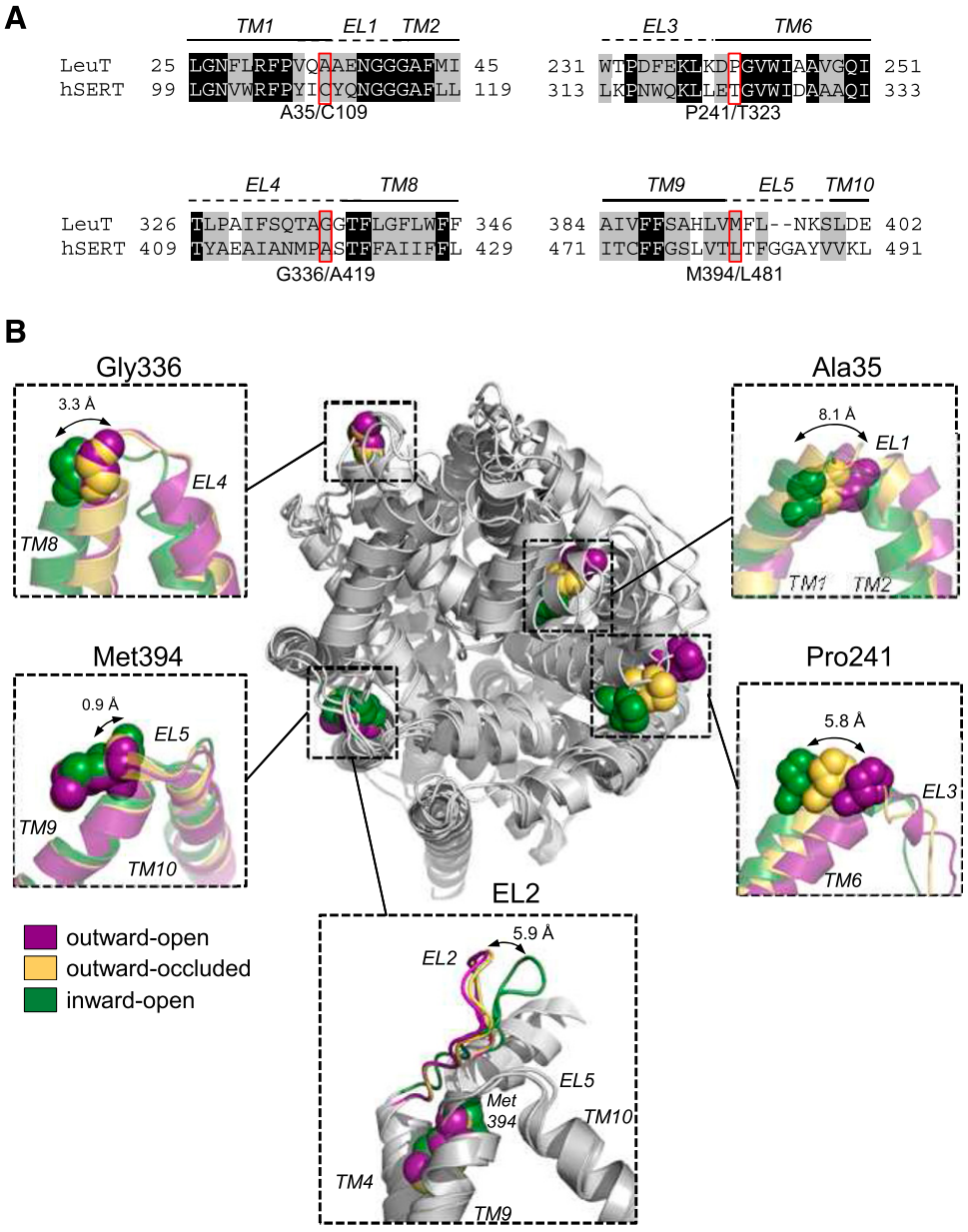

Fig. 6. Movement of reporter positions during predicted state-transitions derived from LeuT structures. (A) Alignment of the amino acid sequence of hSERT and LeuT in the regions surrounding the four reporter positions (indicated by red square; Cys109, Thr323, Ala419, and Leu481; hSERT numbering). Shading indicates amino acid identity (black) or similarity (gray) in terms of physiochemical properties. (B) Structural alignment of X-ray crystal structures of LeuT in different conformational states. Structures of the apo outward-facing open (PDB ID 3TT1), leucine-bound outward-facing occluded (PDB ID 2A65), and apo inward-facing open state (PDB ID 3TT3) are viewed perpendicular from the extracellular side. Inserts show regions in the structures that contain EL1 (upper right), EL3 (lower right), EL4 (upper left), and EL5 (lower left), with the different structures shown in magenta (apo outward-facing open), yellow (substrate-bound outward-facing occluded), and green (apo inward-facing open). The residues in LeuT corresponding to the four fluorescent reporter positions in hSERT are highlighted as spheres and are Ala35 (Cys109 in hSERT) in the top of TM1b, Pro241 (Thr323 in hSERT) in the top of TM6, Gly336 (Ala419 in hSERT) in EL4, and Met394 (Leu481 in hSERT) in EL5. The lower insert shows a zoomed in view of the positions of EL2 and EL5 observed in the membrane plane.

structure. Interestingly, right above EL5 there is a 6-Å displacement of the C-terminal region of EL2 between the outward- and inward-facing conformations of LeuT (Fig. 6C), condensing the structure above EL5 to potentially quench a fluorophore positioned here. However, EL2 is overall poorly conserved between LeuT and hSERT in addition to being 16 residues longer in hSERT (Beuming et al., 2006), and it remains highly speculative whether movement of EL2 relative to EL5 is the source of the quenching until crystal structures of hSERT can reveal the structure and spatial orientation of EL2. The recent dDAT structure does not offer further insight as EL2 in dDAT is even more divergent by containing an additional 47 residues in wild-type dDAT, from which a significant number has been deleted in the crystallized construct (Penmatsa et al., 2013). Still, it is interesting to note that EL2 in hSERT contains multiple aromatic residues, which are excellent fluorescence quenchers. Future studies looking into the role of these for control of fluorescence from the Leu481 reporter position might be warranted.

The consensus idea for inhibitor-bound conformation of *SLC6* transporters is derived mainly from structures of LeuT (Singh et al., 2008) and dDAT (Penmatsa et al., 2013) as well as a LeuT-variant engineered to contain an hSERT-like inhibitor binding site (Wang et al., 2013) crystallized in complex with inhibitors. These overall suggest that inhibitors stabilize a conformation that is almost identical to the apo outward-facing open conformation (Krishnamurthy and Gouaux, 2012), thereby proposing a general mechanism of action in which inhibitors work by arresting the transporter in the outward-facing open conformation while preventing the substrate from binding (Loland, 2015; Penmatsa and Gouaux, 2014). Our VCF data indicate a more complex mechanism as the tested inhibitors all evoke changes in fluorescence from at least three reporter positions. The observation that inhibitor binding is associated with conformational changes in hSERT

indicates that inhibitors stabilize a conformation that is distinctly different from the apo conformation. Furthermore, inhibitors evoke a ΔF that is different from 5-HT ΔF (Fig. 5), indicating the inhibitor-bound state is distinct from the inward-facing conformation. The most striking difference is observed for the Cys109 reporter position, where inhibitor binding lead to unquenching of fluorescence in contrast to 5-HT–evoked quenching. For the Thr323, Leu419, and Ser574 reporter positions, inhibitor ΔF occurs in the same direction as 5-HT ΔF, but of a smaller magnitude. With our assumption that the 5-HT–evoked ΔF represent transitions from an apo outward-facing open conformation to the overall inward-facing conformations, it can be suggested that the smaller inhibitor ΔF represents transition to a state that is in between the apo outward-facing open and inward-facing conformation. Specifically, it might be suggested that inhibitor binding induces conformational changes similar to those that are predicted to occur during the initial transition from the outward-facing open state to the outward-facing occluded state following substrate binding. For fluoxetine and escitalopram, this idea is consistent with docking studies that find that the best binding poses to be in hSERT conformations where the binding site is partly or fully occluded (Andersen et al., 2010, 2014; Koldso et al., 2010). However, transition into a conformation similar to the substrate-bound outward-facing occluded conformation of LeuT would predict the Cys109 reporter position to become quenched as TM1b-EL1 is shifted to a position in between outward open and inward open (Fig. 6B). We observe the opposite for all three inhibitors as inhibitor binding increases Cys109 fluorescence (Fig. 5). Thus, it appears likely that a potential outward-facing inhibitor-bound conformation is distinct from the outward-facing occluded conformation that is observed for substrate-bound LeuT.

Understanding of the protein dynamics underlying inhibitor binding is of importance for future *SLC6* transporter drug development. First, structure-based drug design will be improved with an expanded knowledge base, of which conformational states are stabilized by certain types of inhibitors. Secondly, identification of molecular determinants that control conformational states may allow for the rational design of ligands that target a desired conformational state. This is of interest because seemingly subtle differences in the binding mechanism of *SLC6* inhibitors have been demonstrated to have a profound influence on their in vivo effects. For example, the stimulant dopamine transporter inhibitor cocaine has been suggested to stabilize the outward-facing open conformation, whereas another class of dopamine transporter inhibitors, the benztropines, which lack stimulant effects, stabilize the outward-facing occluded conformation (Beuming et al., 2008; Loland et al., 2008; Kohut et al., 2014). Thus, determination of protein movements upon ligand binding may be an important aspect for understanding the molecular basis for such differences. For these purposes, the present VCF approach may be useful for other *SLC6* transporters to advance understanding of these aspects of transporter molecular pharmacology.

Acknowledgments

The authors thank Drs. Birgit Schiøtt, Lucy Kate Ladefoged, and Stephan Pless for their discussions and valuable comments. The authors also thank Dr. Joseph Lynch for the generous gift of a VCF recording chamber and other advice on the project.

Authorship Contributions

Participated in research design: Söderhielm, Andersen, Munro, Kristensen.

Conducted experiments: Söderhielm, Andersen, Munro, Nielsen, Kristensen.

Performed data analysis: Söderhielm, Andersen, Munro, Nielsen, Kristensen.

Wrote or contributed to the writing of the manuscript: Söderhielm, Andersen, Kristensen.

References

Andersen J, Olsen L, Hansen KB, Taboureau O, Jørgensen FS, Jørgensen AM, Bang-Andersen B, Egebjerg J, Strømgaard K, and Kristensen AS (2010) Mutational mapping and modeling of the binding site for (S)-citalopram in the human serotonin transporter. *J Biol Chem* **285**:2051–2063.

Andersen J, Stuhr-Hansen N, Zachariassen LG, Koldsø H, Schiøtt B, Strømgaard K, and Kristensen AS (2014) Molecular basis for selective serotonin reuptake inhibition by the antidepressant agent fluoxetine (Prozac). *Mol Pharmacol* **85**: 703–714.

Andersen J, Taboureau O, Hansen KB, Olsen L, Egebjerg J, Strømgaard K, and Kristensen AS (2009) Location of the antidepressant binding site in the serotonin transporter: importance of Ser-438 in recognition of citalopram and tricyclic antidepressants. *J Biol Chem* **284**:10276–10284.

Beuming T, Kniazeff J, Bergmann ML, Shi L, Gracia L, Raniszewska K, Newman AH, Javitch JA, Weinstein H, and Gether U et al. (2008) The binding sites for cocaine and dopamine in the dopamine transporter overlap. *Nat Neurosci* **11**: 780–789.

Beuming T, Shi L, Javitch JA, and Weinstein H (2006) A comprehensive structure-based alignment of prokaryotic and eukaryotic neurotransmitter/Na+ symporters (NSS) aids in the use of the LeuT structure to probe NSS structure and function. *Mol Pharmacol* **70**:1630–1642.

Bulling S, Schicker K, Zhang YW, Steinkellner T, Stockner T, Gruber CW, Boehm S, Freissmuth M, Rudnick G, and Sitte HH et al. (2012) The mechanistic basis for noncompetitive ibogaine inhibition of serotonin and dopamine transporters. *J Biol Chem* **287**:18524–18534.

Chen JG, Liu-Chen S, and Rudnick G (1997) External cysteine residues in the serotonin transporter. *Biochemistry* **36**:1479–1486.

Chen JG, Liu-Chen S, and Rudnick G (1998) Determination of external loop topology in the serotonin transporter by site-directed chemical labeling. *J Biol Chem* **273**: 12675–12681.

Cheng Y and Prusoff WH (1973) Relationship between the inhibition constant (K1) and the concentration of inhibitor which causes 50 per cent inhibition (I50) of an enzymatic reaction. *Biochem Pharmacol* **22**:3099–3108.

Felts B, Pramod AB, Sandtner W, Burbach N, Bulling S, Sitte HH, and Henry LK (2014) The two Na+ sites in the human serotonin transporter play distinct roles in the ion coupling and electrogenicity of transport. *J Biol Chem* **289**:1825–1840.

Forrest LR and Rudnick G (2009) The rocking bundle: a mechanism for ion-coupled solute flux by symmetrical transporters. *Physiology (Bethesda)* **24**:377–386.

Gaffaney JD, Shetty M, Felts B, Pramod AB, Foster JD, Henry LK, and Vaughan RA (2014) Antagonist-induced conformational changes in dopamine transporter extracellular loop two involve residues in a potential salt bridge. *Neurochem Int* **73**: 16–26.

Gandhi CS and Olcese R (2008) The voltage-clamp fluorometry technique. *Methods Mol Biol* **491**:213–231.

Jacobs MT, Zhang YW, Campbell SD, and Rudnick G (2007) Ibogaine, a noncompetitive inhibitor of serotonin transport, acts by stabilizing the cytoplasm-facing state of the transporter. *J Biol Chem* **282**:29441–29447.

Kazmier K, Sharma S, Quick M, Islam SM, Roux B, Weinstein H, Javitch JA, and McHaourab HS (2014) Conformational dynamics of ligand-dependent alternating access in LeuT. *Nat Struct Mol Biol* **21**:472–479.

Kohut SJ, Hiranita T, Hong SK, Ebbs AL, Tronci V, Green J, Garcés-Ramírez L, Chun LE, Mereu M, and Newman AH et al. (2014) Preference for distinct functional conformations of the dopamine transporter alters the relationship between subjective effects of cocaine and stimulation of mesolimbic dopamine. *Biol Psychiatry* **76**:802–809.

Koldsø H, Autzen HE, Grouleff J, and Schiøtt B (2013) Ligand induced conformational changes of the human serotonin transporter revealed by molecular dynamics simulations. *PLoS One* **8**:e63635.

Koldsø H, Severinsen K, Tran TT, Celik L, Jensen HH, Wiborg O, Schiøtt B, and Sinning S (2010) The two enantiomers of citalopram bind to the human serotonin transporter in reversed orientations. *J Am Chem Soc* **132**:1311–1322.

Krishnamurthy H and Gouaux E (2012) X-ray structures of LeuT in substrate-free outward-open and apo inward-open states. *Nature* **481**:469–474.

Kristensen AS, Andersen J, Jørgensen TN, Sørensen L, Eriksen J, Loland CJ, Strømgaard K, and Gether U (2011) SLC6 neurotransmitter transporters: structure, function, and regulation. *Pharmacol Rev* **63**:585–640.

Kristensen AS, Larsen MB, Johnsen LB, and Wiborg O (2004) Mutational scanning of the human serotonin transporter reveals fast translocating serotonin transporter mutants. *Eur J Neurosci* **19**:1513–1523.

LeVine MV and Weinstein H (2014) NbIT–a new information theory-based analysis of allosteric mechanisms reveals residues that underlie function in the leucine transporter LeuT. *PLOS Comput Biol* **10**:e1003603.

Li M, Farley RA, and Lester HA (2000) An intermediate state of the gamma-aminobutyric acid transporter GAT1 revealed by simultaneous voltage clamp and fluorescence. *J Gen Physiol* **115**:491–508.

Li M and Lester HA (2002) Early fluorescence signals detect transitions at mammalian serotonin transporters. *Biophys J* **83**:206–218.

Liman ER, Tytgat J, and Hess P (1992) Subunit stoichiometry of a mammalian K+ channel determined by construction of multimeric cDNAs. *Neuron* **9**: 861–871.

Lin F, Lester HA, and Mager S (1996) Single-channel currents produced by the serotonin transporter and analysis of a mutation affecting ion permeation. *Biophys J* **71**:3126–3135.

Loland CJ (2015) The use of LeuT as a model in elucidating binding sites for substrates and inhibitors in neurotransmitter transporters. *Biochim Biophys Acta* **1850**:500–510.

Loland CJ, Desai RI, Zou MF, Cao J, Grundt P, Gerstbrein K, Sitte HH, Newman AH, Katz JL, and Gether U (2008) Relationship between conformational changes in the dopamine transporter and cocaine-like subjective effects of uptake inhibitors. *Mol Pharmacol* **73**:813–823.

Lomize MA, Lomize AL, Pogozheva ID, and Mosberg HI (2006) OPM: orientations of proteins in membranes database. *Bioinformatics* **22**:623–625.

Mager S, Min C, Henry DJ, Chavkin C, Hoffman BJ, Davidson N, and Lester HA (1994) Conducting states of a mammalian serotonin transporter. *Neuron* **12**:845–859.

Malinauskaite L, Quick M, Reinhard L, Lyons JA, Yano H, Javitch JA, and Nissen P (2014) A mechanism for intracellular release of Na+ by neurotransmitter/sodium symporters. *Nat Struct Mol Biol* **21**:1006–1012.

Meinild AK and Forster IC (2012) Using lithium to probe sequential cation interactions with GAT1. *Am J Physiol Cell Physiol* **302**:C1661–C1675.

Meinild AK, Loo DD, Skovstrup S, Gether U, and MacAulay N (2009) Elucidating conformational changes in the gamma-aminobutyric acid transporter-1. *J Biol Chem* **284**:16226–16235.

Penmatsa A and Gouaux E (2014) How LeuT shapes our understanding of the mechanisms of sodium-coupled neurotransmitter transporters. *J Physiol* **592**: 863–869.

Penmatsa A, Wang KH, and Gouaux E (2013) X-ray structure of dopamine transporter elucidates antidepressant mechanism. *Nature* **503**:85–90.

Poulsen MH, Lucas S, Bach TB, Barslund AF, Wenzler C, Jensen CB, Kristensen AS, and Strømgaard K (2013) Structure-activity relationship studies of argiotoxins: selective and potent inhibitors of ionotropic glutamate receptors. *J Med Chem* **56**: 1171–1181.

Pramod AB, Foster J, Carvelli L, and Henry LK (2013) SLC6 transporters: structure, function, regulation, disease association and therapeutics. *Mol Aspects Med* **34**: 197–219.

Quick MW (2003) Regulating the conducting states of a mammalian serotonin transporter. *Neuron* **40**:537–549.

Sandtner W, Schmid D, Schicker K, Gerstbrein K, Koenig X, Mayer FP, Boehm S, Freissmuth M, and Sitte HH (2014) A quantitative model of amphetamine action on the 5-HT transporter. *Br J Pharmacol* **171**:1007–1018.

Schicker K, Uzelac Z, Gesmonde J, Bulling S, Stockner T, Freissmuth M, Boehm S, Rudnick G, Sitte HH, and Sandtner W (2012) Unifying concept of serotonin transporter-associated currents. *J Biol Chem* **287**:438–445.

Singh SK, Piscitelli CL, Yamashita A, and Gouaux E (2008) A competitive inhibitor traps LeuT in an open-to-out conformation. *Science* **322**:1655–1661.

Sørensen L, Andersen J, Thomsen M, Hansen SM, Zhao X, Sandelin A, Strømgaard K, and Kristensen AS (2012) Interaction of antidepressants with the serotonin and norepinephrine transporters: mutational studies of the S1 substrate binding pocket. *J Biol Chem* **287**:43694–43707.

Sørensen L, Strømgaard K, and Kristensen AS (2014) Characterization of intracellular regions in the human serotonin transporter for phosphorylation sites. *ACS Chem Biol* **9**:935–944.

Tavoulari S, Forrest LR, and Rudnick G (2009) Fluoxetine (Prozac) binding to serotonin transporter is modulated by chloride and conformational changes. *J Neurosci* **29**:9635–9643.

Wang H, Goehring A, Wang KH, Penmatsa A, Ressler R, and Gouaux E (2013) Structural basis for action by diverse antidepressants on biogenic amine transporters. *Nature* **503**:141–145.

Yamashita A, Singh SK, Kawate T, Jin Y, and Gouaux E (2005) Crystal structure of a bacterial homologue of Na+/Cl–dependent neurotransmitter transporters. *Nature* **437**:215–223.

Zhang YW and Rudnick G (2006) The cytoplasmic substrate permeation pathway of serotonin transporter. *J Biol Chem* **281**:36213–36220.

Zhao C, Stolzenberg S, Gracia L, Weinstein H, Noskov S, and Shi L (2012) Ion-controlled conformational dynamics in the outward-open transition from an occluded state of LeuT. *Biophys J* **103**:878–888.

Address correspondence to: Anders S. Kristensen, Department of Drug Design and Pharmacology, University of Copenhagen, Universitetsparken 2, DK-2100 Copenhagen, Denmark. E-mail: ask@sund.ku.dk